Properties and Reactivity toward Water of A Type Carbonated Apatite and Hydroxyapatite Surfaces

(Article begins on next page)

02 February 2025

Properties and Reactivity Towards Water of A-Type Carbonated Apatite and Hydroxyapatite Surfaces

Francesca Peccati,[*,†] Cristina Bernocco,[‡] Piero Ugliengo,[‡] and Marta Corno[*,‡,¶]

†*Universitat Autònoma de Barcelona, Departament de Química, Campus UAB, 08193 Bellaterra, Spain*

‡*Università degli Studi di Torino, Dipartimento di Chimica, Via P. Giuria 7, 10125 Torino, Italy*

¶*Current address: Università degli Studi del Piemonte Orientale "Amedeo Avogadro", Dipartimento di Scienze e Innovazione Tecnologica, Viale Teresa Michel, 11, 15121 Alessandria, Italy*

E-mail: francesca.peccati@uab.cat; marta.corno@uniupo.it

Phone: +34935812173; +390131360418

Abstract

Hydroxyapatite (HA) and carbonated apatite (CAp) constitute the mineral part of biological hard tissue and are key materials in dental implants and bone regeneration. This work provides a density functional theory study of the static and dynamic properties and reactivity towards water of three families of HA and CAp surfaces, namely the (001), (010) and (101) surfaces. For clean materials, surface energy, dipole moment across the slab and vibrational features of the CO_3^{2-} group in CAp are compared with either the same surface property of HA, or with the bulk feature. The full substitution of OH^- groups by CO_3^{2-} in CAp affects water adsorption features significantly

compared to HA. When CO_3^{2-} is not directly exposed at the surface ((001) and P-rich (010) surfaces) water binding energy is increased/decreased by less than 25% compared to the values for the corresponding HA surfaces. For the CAp Ca-rich (010) surface, in which the CO_3^{2-} group in direct contact with water, the binding energy shows a 50% increase. For both the HA and CAp (010) stoichiometric surfaces, water is spontaneously dissociated with the resulting OH^- ion shared between three surface Ca ions.

Introduction

Apatites are phosphate minerals with the general formula $Ca_{10}(PO_4)_6(X)_n$, where X stands for a number of anions, including F^-, Cl^-, OH^- and CO_3^{2-}. The composition of these minerals is not fixed, yielding a spectrum of different structures according to substitution. Hydroxyapatite $[Ca_{10}(PO_4)_6(OH)_2]$ (HA) and carbonated hydroxyapatite $[Ca_{10}(PO_4)_{6-2y}(OH)_{2-2x}(CO_3)_{x+3y}]$ (CHA) are the main mineral component of biological hard tissues, and have been the object of extensive study in the field of bone regeneration and dental implants.[1–5] Two different anionic substitutions are originated: carbonate can replace phosphate (B-type case) or hydroxyl groups (A-type). Mixed AB-types are also found in bone minerals.[6]

CHA can be seen as a derivative of HA resulting from CO_3^{2-} incorporation. Moreover, when CO_3^{2-} completely replaces OH^- ions in the lattice, the resulting mineral $[Ca_{10}(PO_4)_6(CO_3)]$, with a CO_3^{2-} content of 5.82 wt%, takes the name of fully carbonated A-type apatite (herein CAp), which is the object of this work.[7–10] HA and CAp can be seen as the extremes of a continuous range of structures with varying OH^-/CO_3^{2-} ratio, which includes biological hard tissues, whose CO_3^{2-} content stays in the range 2-8 wt% according to bone location and species for mammals.[11] Remarkably, while the Raman spectra of apatite in enamel are characterized by the $O-H$ stretching modes of the hydroxyl group in the apatitic structure, some bone apatite has been shown to be entirely hydroxyl groups free.[12] On the other hand, the presence of trigonal-planar CO_3^{2-} groups is clearly recognizable in the IR spectra of both bone and enamel, indicating that HA alone is not as good a model for biological hard tissue

as a combination of HA and CAp.

The role of the carbonate ion in hydroxyapatite has gained much interest since it has been proven to be relevant for different pathologies of human tissues, such as dental caries[13,14] and even breast cancer.[15] For applications in bone tissue engineering, the design of carbonate substituted hydroxyapatite ceramics is very promising[16] due to the inductive effect on osteoclastogenesis in proximity of the implant, allowing for highly resorbable biomaterials.[17] Cationic substitutions are studied as well for A-type carbonated hydroxyapatite, such as Zn-doping, reaching a chemical composition close to that of natural biological apatite.[18] The effect of carbonate concentration in controlling bone mineral morphology has been considered and explained for the B-type carbonated hydroxyapatite in a recent combined experimental and computational work by Deymier et al.[11] The authors have proposed a mechanism elucidating how carbonate substitution affects morphology, shedding light on the key role of carbonation. Actually, computational techniques have revealed as a fundamental tool for these investigations, especially when related to surface processes. Indeed, a large number of studies have applied theoretical methods to pure and substituted hydroxyapatite, both by classical molecular dynamics[19,20] and quantum-mechanical techniques.[21–23]

In previous works some of us have simulated extensively both bulk and surface properties of HA,[24–29] and more recently the bulk properties of CAp.[30–33] The study of surfaces of biological materials is particularly relevant as these contribute to the complex interface with biological tissue and fluids. Even more importantly, as the main application of HA and CAp is in bone regeneration, surface properties and reactivity are crucial to understand the response of the biomaterial implanted in a living body.

The aim of this work is to model the structural and vibrational properties of three families of CAp surfaces, (001), (010) and (101), and compare them with the corresponding HA ones, the ultimate goal being to assess how does carbonate substitution affect the properties of the material. Concerning surface reactivity, a first computational exploration has been carried out, again comparing HA and CAp, by considering the reactivity of (001) and (010) surfaces

3

towards water molecules. The reactivity of the (101) surface is more complex compared to the other surfaces as we showed[29] that for HA, up to two water molecules are dissociatively chemisorbed. As we are interested in the limit of very low H_2O coverage, the (101) surface will be considered in future work when dealing with the comparison between HA and CAp at water monolayer.

Computational methods

Static calculations

Static calculations were performed with a development version of the CRYSTAL14 code, using the hybrid B3LYP functional.[34,35] With B3LYP we are not taking dispersive (London) interactions into account. This is fully justified particularly for a comparative study like the present one, as we recently showed that its role when dealing with water adsorption at HA surfaces is not crucial, as the interaction is dominated by charge-dipole interaction, well accounted for by plain B3LYP.[29] The all-electron Gaussian basis set, already used in previous related works, is as follows: 86-511G(2d) for calcium, 85-21G(d) for phosphorus, 6-31G(d) for oxygen and 6-21G(d) for carbon.[30–32] This methodology has already been applied to the study of mixed A-type and B-type carbonated hydroxyapatite surfaces by Ulian et al.[22] Truncation criteria for the Coulomb and Hartree-Fock exchange series were set to 10^{-6} (ITOL1, ITOL2, ITOL3, ITOL4) and 10^{-16} (ITOL5). Geometry optimization was carried out keeping the unit cell parameters fixed to optimum bulk values, and surface energies were not corrected for the basis set superposition error to ensure continuity with the previous works on hydroxyapatite. A sample SCF section of the CRYSTAL input employed is reported in the supporting information.

The Hamiltonian matrix was diagonalized at 10 k-points in the first Brilloiun zone. Model surfaces were constructed using the slab model, yielding a series of thin films of definite thickness, which will be described in detail in the next section. This, in combination with

the use of a Gaussian type basis set, allows the construction of two-dimensional models where the direction perpendicular to the slab surface is truly non-periodic (no replicas). The interaction energies presented for water molecules physisorbed on surfaces include the counterpoise correction for the basis set superposition error.[36,37] Harmonic frequencies were computed for the carbonate group only, considered as an independent fragment within the structure.

Molecular dynamics simulations

DFT molecular dynamics simulations were performed using the CP2K package, version 2.6.2.[38,39] Periodic molecular dynamics simulations of selected surface models were performed in the NVT (isothermal) ensemble. In order to avoid unphysical interactions between adjacent replicas along the non-periodic direction (z), the simulation box was set with a 50 Å height along z. The largest model taken into account in these simulations is ~ 24 Å thick, which leaves at least a ~ 26 Å distance between replicas, enough to prevent any interaction. The calculations were performed in Gamma-point. The PBE functional was employed, with a Gaussian split-valence double zeta basis set with polarization functions for valence electrons, and the Goedecker-Teter-Hutter pseudopotentials for core electrons.[40,41] Alongside the Gaussian basis set, CP2K uses an auxiliary plane wave basis set for which the cutoff was set to 400 Ry. A CSVR (Canonical Sampling through Velocity Rescaling) thermostat with a time constant of 25 fs was employed to control the temperature of the simulation, which was set to 300 K.[42] Sample force evaluation and molecular dynamics blocks of the CP2K inputs are reported in the ESI.

Results and discussion

CAp (001), (010) and (101) surface models

With the optimized CAp bulk[32] as the starting point (Figure S1 of ESI), three types of surface models were cut. These are identified by the (hkl) crystal planes defining the cutting direction, as reported in Figure 1. The corresponding CIF files are available in the ESI. As highlighted by the orientation of CO_3^{2-} ions, the three cuts expose different atomistic terminations.

●C	●O	●P	●Ca

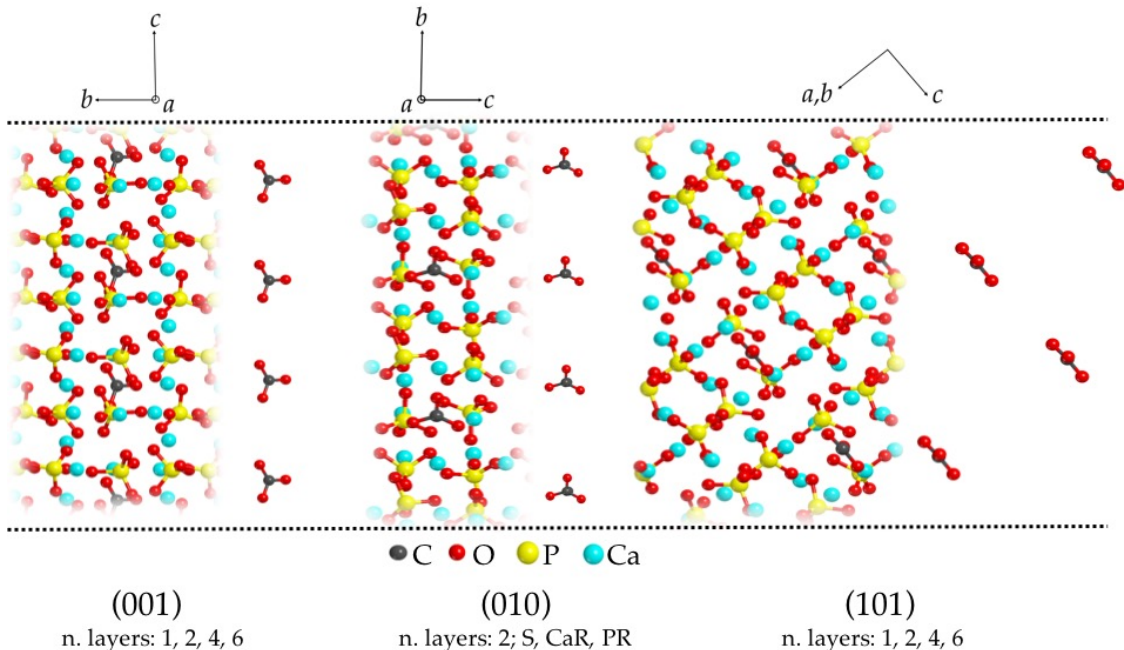| (001) | (010) | (101) |
| n. layers: 1, 2, 4, 6 | n. layers: 2; S, CaR, PR | n. layers: 1, 2, 4, 6 |

Figure 1: Cutting direction of the bulk of CAp yielding the surface models of this work, with indication of the orientation of carbonate ions. The dotted line defines in all cases the cut direction (z).

Cutting the bulk along the (001) and (101) directions four slabs were constructed, with different thickness corresponding to 1, 2, 4 and 6 bulk unit cells. (Figures S2 to S6 of ESI). Cutting along the (010) direction, on the other hand, yields three types of surfaces: a stoichiometric one (S, Ca/P ratio 1.67), and two non-stoichiometric ones, P-rich (PR, Ca/P ratio 1.62) and Ca-rich (CaR, Ca/P ratio 1.71) respectively (Figure S7 and S8 of ESI). Non-

stoichiometric means that the formula unit of the slab unit cell cannot be expressed as an integer multiple of the bulk unit cell, resulting in a different composition (bulk Ca/P ratio 1.67). For the S surface, a bilayer was cut. With the aim of constructing non-stoichiometric slabs of similar thickness, a PR model was constructed including two CO_3^{2-} ions in the unit cell, and a CaR one with three CO_3^{2-} ions. Figure 2 reports the Wulff construction of HA (space group $P6_3$, Figure 2a) and CAp (space group $P\bar{3}$, Figure 2b), in which the computed morphologies resulted from the surface energy values calculated as described in the methodology section.
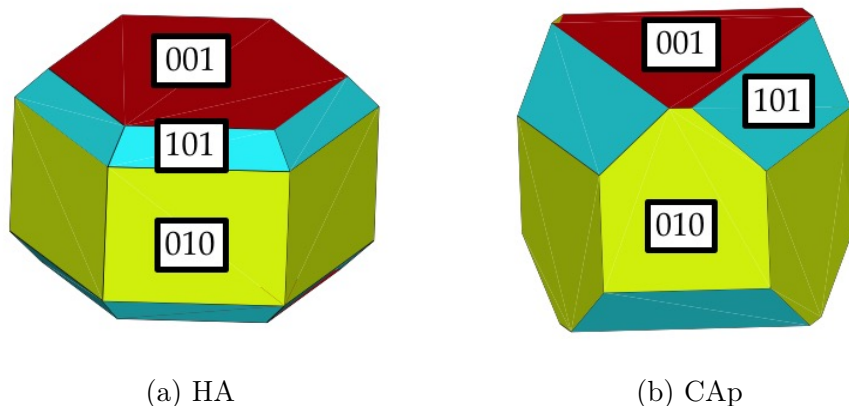

(a) HA   (b) CAp

Figure 2: Wulff construction of HA and CAp.

In the following sections, the properties of these three surfaces will be presented. Since an important geometrical reorganization is expected after the cut, slab models have been optimized relaxing atomic position, but keeping cell parameters fixed to bulk values. In order to assess the modifications brought by surface cutting, the harmonic frequencies of CO_3^{2-} ions were computed. In particular, the shift between slab and bulk values of the two asymmetric stretching frequencies of CO_3^{2-} (Figure 3) can bring information on the surrounding of carbonate in the different surface models.
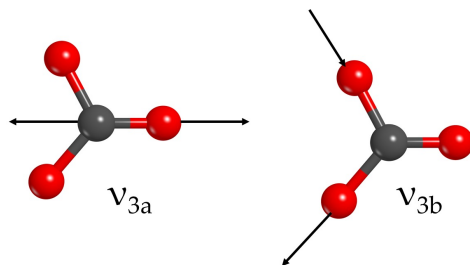
Figure 3: Asymmetric stretching modes of the carbonate ion.

(001) and (101) surfaces

Four models of (001) were built, with thickness ranging from 1 to 6 bulk unit cells. Figure 4a reports the optimized geometry of one of these models, the tetralayer. As highlighted, the heavy geometrical reorganization at the surface is reflected in the spatial arrangment of CO_3^{2-}. Indeed, CO_3^{2-} ions closer to the slab faces (labelled E) are rotated compared to the bulk orientation, which is maintained by the internal carbonates (labelled I). This rotation, which is of $\sim 46°$ independently of slab thickness (see Figure S9 of ESI), confirms that CO_3^{2-} is an extremely mobile group within the material.

With the aim of understanding how carbonate substitution affects the properties of the material, we compared CAp (001) surfaces with the corresponding HA ones. In particular, surface energy and dipole moments have been taken into account. Surface energy has been computed according to eq. 1.
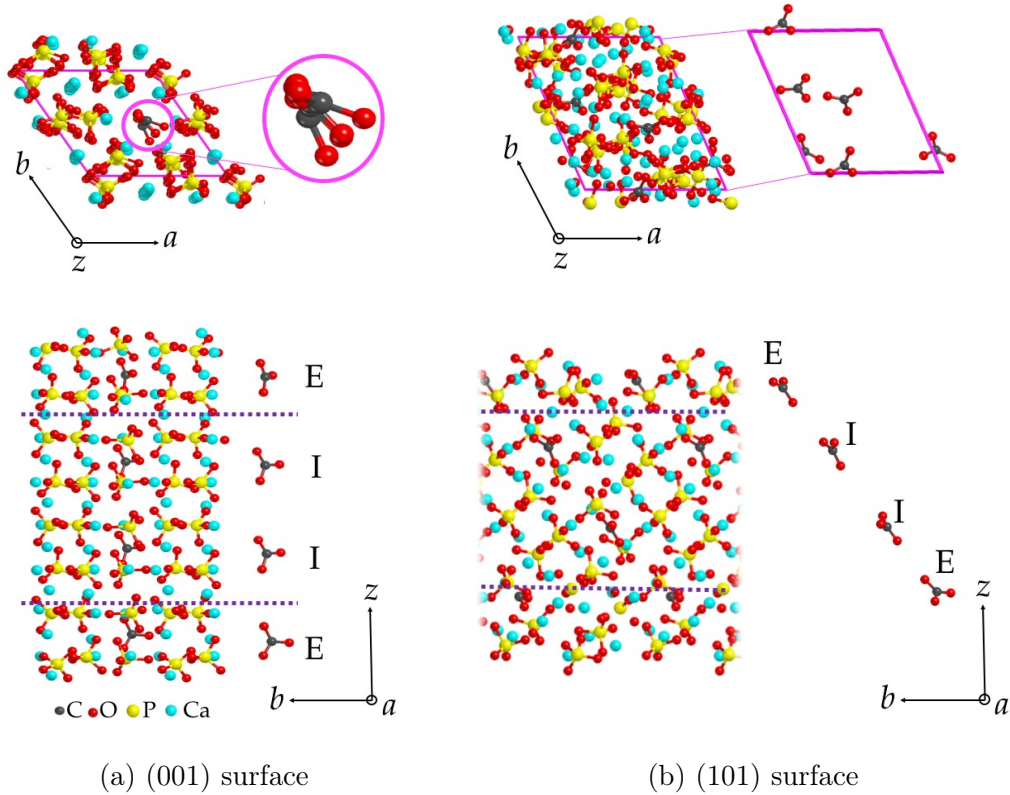
(a) (001) surface   (b) (101) surface

Figure 4: Top and side view of the optimized CAp (001) and (101) surfaces, with labeling of the CO_3^{2-} groups according to their position perpendicular to the cutting direction. E identifies external and I internal CO_3^{2-} groups. The dotted lines separate the internal zones from the external ones.

$$E_{surf} = \frac{E_{sN} - N \cdot E_{bulk}}{2A} \tag{1}$$

where E_{sN}, N, E_{bulk} and A are the energy of the slab unit cell, thickness of the slab model expressed as number of bulk unit cells, the bulk unit cell energy and the slab unit cell area respectively. Since cell parameters were not optimized, the value of A is constant for all (001) slab models. Surface energy converges rapidly to a value of 0.90 J m⁻² (see Figure S10 of ESI), which is higher than the value of 0.75 J m⁻² for hydroxyapatite at B3LYP level and with a slightly more extended basis for the oxygen atoms (511111-411G(d)) compared to the present one.[29] As the E_{surf} datum for hydroxyapatite refers only to the (001) tetra-layer slab this does not allow to compare the surface property evolution of CAp with slab thickness. To

that purpose, we resort to data computed for the HA (001) surface using a pseudo-potential for the core electrons of Ca ions and double zeta quality basis set for the other atoms as reported in Table 1 (please note that we refer to the value computed for the optimized HA (001) slab as reported in Table 3 under the "Relaxed" header of Reference.[27])

Table 1 reports a comparison of HA and CAp in terms of thickness and dipole moment of (001) surface models. While carbonate substitution does not essentially affect surface thickness, it increases significantly the dipole moment, both before and after geometry relaxation. This marked difference can be attributed the carbonate ion, which has high mobility and whose spatial arrangements lead to multiple energetically equivalent minima.[32]

Table 1: Thickness τ (Å) and surface energy E_{surf} for relaxed CAp and HA surfaces, and dipole moment μ (D) across the slab for unrelaxed and relaxed HA and CAp (001) surfaces. Data for HA taken from Ref.[27]

n. layers	τ		E_{surf}		μ-CAp		μ-HA	
	CAp	HA	CAp	HA	Unrelaxed	Relaxed	Unrelaxed	Relaxed
1	6.9	6.6	0.92	-	0.64	-0.14	-	-
2	13.8	13.2	0.90	1.04	1.27	0.03	0.38	0.02
4	27.5	27.0	0.90	1.05	2.51	0.16	0.39	0.07
6	41.3	40.4	0.90	1.05	3.75	0.64	0.41	0.13

Similar properties are observed for surface (101) (Figure 4b). As already reported for HA, the (101) surface cut from the bulk exhibits channel anions (OH$^-$ in HA and $CO_3{}^{2-}$ in CAp) running diagonally across the slab model, resulting in a high dipole moment.[26] Reconstruction of this surface involves important reorientation of these anions, yielding values of dipole moment that are higher than those of the (001) surface, as shown in Table 2. These results have been compared with those of the (101) HA bilayer: a thickness of 12.05 Å, very similar to the CAp bilayer, a surface energy of 1.65 J m^{-2}, significantly higher than that of CAp, and a dipole moment that vanishes with surface relaxation, unlike what reported for CAp.[29] The latter represents an important difference between the two materials: in HA the dipole moment across the slab vanishes owing to a rotation of the terminal exposed hydroxyl groups of the slab, which assume a spatial configuration that is essentially perpendicular

to that of the remaining internal OH^- groups and effectively cancel out the dipole moment generated by the internal hydroxyls. This cannot take place in CAp owing to the nature of A-type substitution: when a single CO_3^{2-} group replaces two OH^- ones, the terminal groups are no longer completely exposed to the surface, and thus their geometrical reorganization is hindered by the surrounding groups and is much less effective in vanishing the dipole moment.

Table 2: Thickness τ (Å), dipole moment μ (D) and surface energy E_{surf} (J m^{-2}) of the relaxed (101) and CAp surface.

n. layers	τ	E_{surf}	μ
1	6.3	1.04	0.01
2	11.9	1.02	-0.21
4	22.3	1.05	-1.75
6	33.1	1.04	-2.08

(010) surfaces

Three models of (010) surface were constructed, the difference between them lying in the type of cut. If the bulk of CAp is oriented perpendicular to the (010) direction (Figure 5), two types of layers can be recognized: A-type layers, $Ca_3(PO_4)_3$, and B-type layers, $Ca_4(PO_4)_2CO_3$, in such a way that the bulk structure is a repetition of the ABB unit $(Ca_{10}(PO_4)_6(CO_3))$, corresponding to the unit cell. The ABA termination yields a stoichiometric surface, the BAA a P rich one, and the AAB a Ca rich one (Figure 5).
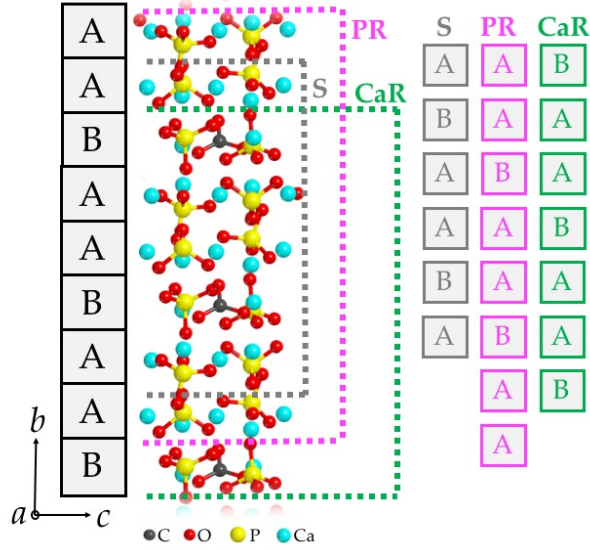
Figure 5: Cuts yielding the three models of (010) surface, stoichiometric (S), P rich (PR) and Ca rich (CaR).

Concerning surface energy, for the stoichiometric slab eq. 1 can be applied, yielding a value of 1.07 J m^{-2} to be compared with the value of 1.34 J m^{-2} computed for the stoichiometric HA (100) surface.[29] Evaluation of surface energies of non-stoichiometric slabs is more complex, as it involves modification of eq. 1 to account for the layers that the model lacks or has in excess compared to the stoichiometric one. By applying the same procedure already followed by some of us for the corresponding hydroxyapatite surfaces,[29] once that the chemical potential of the A-type layer (μ_A) is known, surface energies can be computed according to the following equations.

$$E_{surf}(CaR) = \frac{E_{CaR} + 2 \cdot \mu_A - 3 \cdot E_{bulk}}{2A} \tag{2}$$

$$E_{surf}(PR) = \frac{E_{PR} - 2 \cdot \mu_A - 2 \cdot E_{bulk}}{2A} \tag{3}$$

To evaluate μ_A, two reference systems are employed:

i) A first value, μ_1, can be computed from the decomposition of CAp into calcium phosphate and calcium carbonate:

$$Ca_{10}(PO_4)_6(CO_3) \rightarrow CaCO_3 + 3[Ca_3(PO_4)_2]$$

$$\mu_1 = \frac{1}{3}[E_{CAp} - E_{CaCO_3}] \tag{4}$$

Where E is the electronic energy per formula unit.

ii) A second value, μ_2, can be computed from the most stable form of calcium phosphate, β-tricalcium phosphate (β-TCP):

$$\mu_2 = E_{\beta-TCP} \tag{5}$$

μ_1 and μ_2 values define the window of stability of (010) non-stoichiometric surfaces, according to:

$$\mu_1 < \mu_A < \mu_2 \tag{6}$$

Indeed, if $\mu_A < \mu_1$, the surface decomposes into $CaCO_3$ and $Ca_3(PO_4)_2$. If, on the other hand, $\mu_A > \mu_2$, precipitation of β-TCP prevents surface formation.

Limiting values of surface energies computed with μ_1 and μ_2 are reported in Table 3. Values for HA are taken from ref.[29] and indicate that HA and CAp have a very similar behavior, suggesting that carbonate substitution does not affect significantly the surface energy.

Table 3: (010) Surface energies of HA and CAp in J m^{-2} and dipole moment μ (D) of CAp.

	$E_{surf}(\mu_1)$		$E_{surf}(\mu_2)$		μ
Surface	HA	CAp	HA	CAp	CAp
CaR	0.99	1.11	1.14	1.17	-0.12
PR	1.12	1.04	0.99	0.98	0.87

While for the P rich termination CO_3^{2-} ions are buried below two A-type layers, for the Ca rich termination they are located in the outmost layer. The stoichiometric surface, in turn, involves an intermediate situation between the two non-stoichiometric ones with an E_{surf} of 1.07 J m^{-2}, very close to those reported in Table 3.

Surface vibrational features

As already anticipated, we focused exclusively on the CO_3^{2-} features computed in the harmonic approximation. This approximation of the carbonate group as independent within the lattice is justified by its extreme mobility.[32] The different local environment perceived by the carbonate ions in the three situations is reflected in the vibrational frequencies reported in Table 4. Carbonates are classified according to their distance from the two faces of slab models. E stands for external, and indicates the two CO_3^{2-} groups closer to these faces, while I, which stands for internal, refers to CO_3^{2-} ions that are buried inside the slab (Figure 4).

Table 4: Asymmetric stretching frequencies of CO_3^{2-} in the models of (001), (010) and (101) CAp surfaces. Values of ν_{3a} and ν_{3b} are reported as differences relative to bulk values ($\nu_{3a,bulk}$ = 1516 cm⁻¹, $\nu_{3b,bulk}$ = 1602 cm⁻¹, $\nu_{3a} - \nu_{3b}$ = 86 cm⁻¹). E stands for external CO_3^{2-}, I for internal. Multiple entries in the same cell correspond to different carbonate groups in the same position (external or internal) along the non-periodic direction. For the (001) and (101) surfaces results are given as a function of the number of layers. Concerning (010) surfaces, the models of S and PR present two CO_3^{2-} groups only, which are therefore labelled as external being the ones closer to the vacuum. In the CaR model, three CO_3^{2-} groups are present, the two most exposed being labeled as E and the internal one as I.

	Surface	1	2	4	6	8	Surface	1	2	4	6
E $\nu_{3a} - \nu_{3a,bulk}$	(001)	12	-34/-24	-30/-21	-21/-29	-27/-21	(101)	-163	-99/-5	-118/-170	-122/-4
E $\nu_{3b} - \nu_{3b,bulk}$	(001)	-28	-34/-31	-26/-32	-33/-26	-24/-30	(101)	108	24/-45	55/-90	51/35
E $\nu_{3b} - \nu_{3a}$	(001)	46	100/78	90/74	74/89	87/75	(101)	357	209/46	259/166	259/125
I $\nu_{3a} - \nu_{3a,bulk}$	(001)	-	-	7/10	13/16	12/18	(101)	-	-	-90/18	4/7
I $\nu_{3b} - \nu_{3b,bulk}$	(001)	-	-	0/1	-4/-1	-3/1	(101)	-	-	-95/-8	-12/2
I $\nu_{3b} - \nu_{3a}$	(001)	-	-	77/78	69/69	67/79	(101)	-	-	81/69	81/81

	Surface		Surface		Surface			Surface	
E $\nu_{3a} - \nu_{3a,bulk}$	(010)S	-96/-69	(010)CaR	-114/-113	(010)PR	16/5	I $\nu_{3a} - \nu_{3a,bulk}$	(010)CaR	2
E $\nu_{3b} - \nu_{3b,bulk}$	(010)S	14/2	(010)CaR	31/20	(010)PR	11/4	I $\nu_{3b} - \nu_{3b,bulk}$	(010)CaR	-5
E $\nu_{3b} - \nu_{3a}$	(010)S	196/157	(010)CaR	230/220	(010)PR	81/81	I $\nu_{3b} - \nu_{3a}$	(010)CaR	78

For the (001) surface, results indicate that external CO_3^{2-} groups undergo a $\sim$ 27 cm⁻¹ bathochromic shift compared to bulk values, while internal ones yield values closer to bulk ones. This is an interesting result, considering that in our (001) models CO_3^{2-} ions are not fully exposed, but protected by a layer of phosphate and calcium ions. This indicates that the stretching frequencies are sensitive enough to be used as probes for surface structure. The only exception to this trend is offered by the monolayer, that shows a hypsochromic shift for ν_{3a}. This peculiar behavior may be attributed to the extreme thinness of this model,

which is not representative of the real surface structure.

While CO_3^{2-} groups of the (010) P rich slab present a signature frequency that is essentially identical to that of bulk carbonates, CO_3^{2-} ions of the Ca rich surface present bathochromic shifts larger than 100 cm^{-1} for ν_{3a} compared to bulk values, highlighting the lesser spatial constraint of groups exposed to the surface. The same effect, although less pronounced, is observed for the stoichiometric (010) surface. Furthermore, it is interesting to notice that the two signature vibrational frequencies are affected differently by exposure to the surface.

The (101) surface shows a markedly higher frequency shift of external CO_3^{2-} ions to that of the (001) surface. This is attributed to the different position of these groups, which are fully exposed in the (101) surface, and thus in a chemical environment that is very different from the bulk one. It also interesting to stress how the two modes are not affected by exposure to the surface to the same extent, with mode ν_{3a} undergoing more significant variations than mode ν_{3b}. This difference is explained when looking at the vibrational mode within the surface structure (Figure 6).
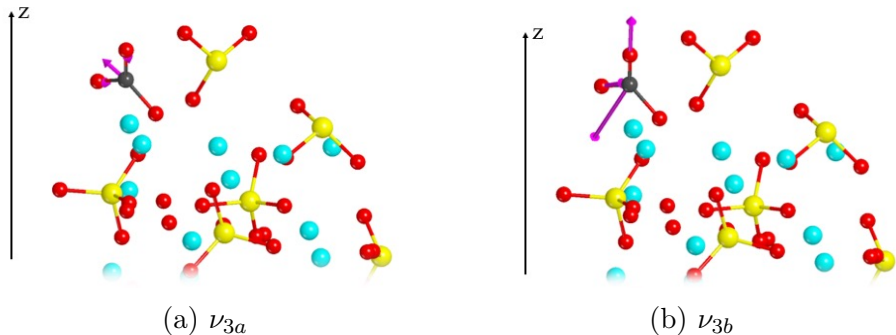

(a) ν_{3a} (b) ν_{3b}

Figure 6: ν_{3a} and ν_{3b} stretching modes of (101) surface CO_3^{2-} ions. Arrows represent the vibrational mode.

Mode ν_{3a} (Figure 6a) involves an outward atomic displacement, pointing at the empty space of the non-periodic direction and with negligible interactions with other groups of the surface. On the contrary, mode ν_{3b} (Figure 6b) has an important out-of-plane bending

contribution, pointing towards the interior of the surface model, which is constrained by the lower groups of the slab model. These variations, which are dependent on the chemical environment of $CO_3{}^{2-}$ and on its orientation within the apatite channel, are only representative of a specific atomic configuration, and only an average over all possible configurations is expected to be representative of the behavior of real CAp surfaces.

Water reactivity at the (001) and (010) surfaces

This sections compares the properties of water adsorption at zero-coverage limiting value (one water molecule per surface unit cell) of the (001) and (010) stoichiometric surfaces of HA and CAp, leaving aside the (101) one. As already anticipated, this choice was dictated by the fact that the HA (101) surface is highly reactive towards water adsorption and their properties cannot be described well at low water coverage.[29] For this reason, water adsorption at the (101) CAp surface was not considered here and will be addressed in detail in future work.

As we are considering an extremely low water coverage, the following results provide only a preliminary overview of water reactivity at the CAp surfaces and cannot therefore considered representative of the behavior of the surface in a biological environment, which involves a much higher level of complexity and will be addressed elsewhere.

Static simulations

In order to rationalize the presentation of results, surface calcium ions are labeled as shown in Figures 7a, 7c and 8, according to what reported by Corno et al.[25,43] These cations are directly involved in water adsorption through electrostatic interactions with the oxygen atom of water, while phosphate groups can interact with the hydrogen atoms, either accepting the proton resulting from the water O−H bond cleavage, or just by forming an hydrogen bond with the water molecule.

Previous studies by Corno and coworkers analyzed the evolution of water adsorption on

HA surfaces as a function of water loading.[25,29] On hydroxyapatite stoichiometric (001) surfaces, water molecules are physisorbed at the Ca1 site (Figure 7a), with an interaction energy of -102 kJ mol^{-1} per water molecule (see B3LYP ΔE^C values of Table 2 in Ref[29]). A similar behavior was observed for CAp, with an interaction energy of -119 kJ mol^{-1} (Figure 7b). Interestingly, the present value is definitely higher than the value of 86 kJ mol^{-1} computed by Ulian et al.[23] for water adsorbed on the Ca ion of the mixed AB defective apatite. As in the hydroxyapatite case, phosphate groups are involved in the binding interaction via hydrogen bonds. This confirms, in agreement with CO_3^{2-} vibrational results, that as far as surface (001) is concerned, carbonate substitution does not affect significantly surface properties. Ca3 ions (Figure 7a) are known to be only weak interaction sites for water in HA,[29] and were therefore not considered in this study.
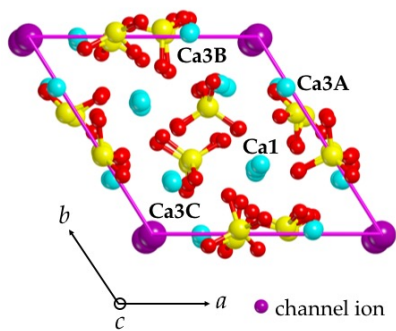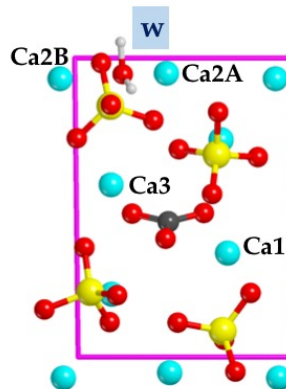
(a) HA (001): labeling of Ca ions.
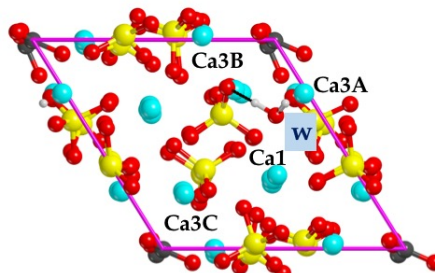
(b) CAp (001): physisorption on Ca1.
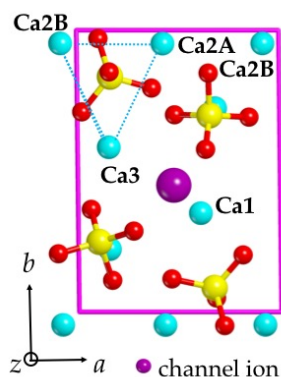
(c) HA (010) S: labeling of Ca ions.
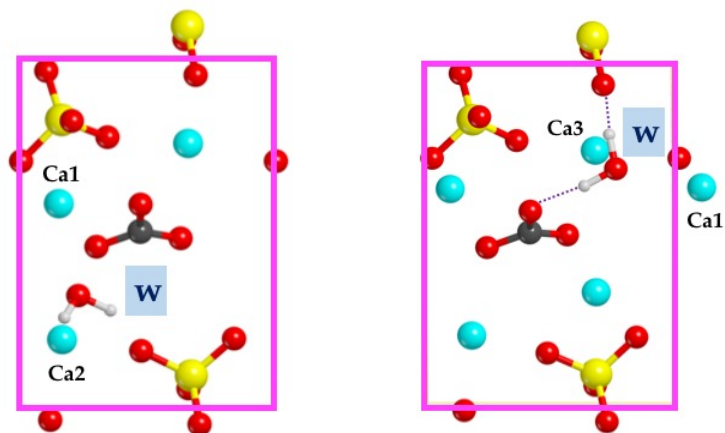

(d) CAp (010) S: physisorption on Ca2.

Figure 7: Physisorption of one water molecule at the (001) and (010) stoichiometric surfaces of CAp, top view.

As for the stoichiometric (S) (010) surface, water reactivity on HA has been characterized in detail in a previous work,[25] with results indicating clearly that Ca1 (Figure 7c) is the only site promoting adsorption of water in molecular form. On Ca2 and Ca3 type ions, water dissociates in a barrierless manner, and the final configuration involves sharing of the OH^- anion between three adjacent calcium ions and protonation of a nearby phosphate. The lack of dissociation on Ca1 has been attributed just to this OH^- sharing feature, which cannot be achieved on Ca1 because the latter does not have another cation nearby to be involved in the sharing.[25]

For the S (010) surface, a similar behavior is expected for HA and CAp. This assumption is based on the observation that the channel ion (OH^- in HA and CO_3^{2-} in CAp) is not

involved in the dissociation, at least in this first stage (Figure 7c). Our static calculations, however, located a series of minima for CAp corresponding to physisorbed water, interacting not only with Ca1, but also with Ca2 (Figure 7d). To verify if this difference from HA is real or just an artefact, we performed short molecular dynamics simulations to study the adsorption of water on (010) CAp surfaces, reported in the next section.

Concerning HA (010) non-stoichiometric surfaces, previous studies showed that water is physisorbed on both, with an interaction energy of -102.6 kJ mol^{-1} on the Ca-rich and of -135.4 kJ mol^{-1} on the P-rich surface (see B3LYP ΔE^C values of Table 2 in Ref[29]). A similar behavior was observed for CAp, with water being physisorbed through electrostatic interactions between the oxygen of water and calcium ions, and hydrogen bonds involving phosphate groups. Concerning the Ca-rich surface, we located two minima, shown in Figure 8a and 8b. In the first of these structures water is almost equally shared between two adjacent calcium ions, Ca1 and Ca2, with an interaction energy of -80.4 kJ mol^{-1}. The second structure also presents a sharing, this time between Ca1 and Ca3. In this case, however, the Ca−O distance for Ca1 is significantly shorter than that of Ca3, resulting in an interaction energy of -152.2 kJ mol^{-1}. This higher value is not surprinsing because Ca1 is the most exposed among the calcium ions, and thus provides the strongest electrostatic contribution to the adsorption. An interesting feature of this surface is that it exposes the carbonate ion, providing a structure that is essentially different from the corresponding one of HA. In Figure 8b it is shown that the carbonate group is directly involved in water adsorption acting as a hydrogen bond acceptor. Overall, CAp seems to provide a stronger binding interaction than HA (-152.2 kJ mol^{-1} vs -102.6 kJ mol^{-1}).

(a) Ca1-O 2.67 Ca-O 2.60   (b) Ca1-O 2.37 Ca3-O 2.56
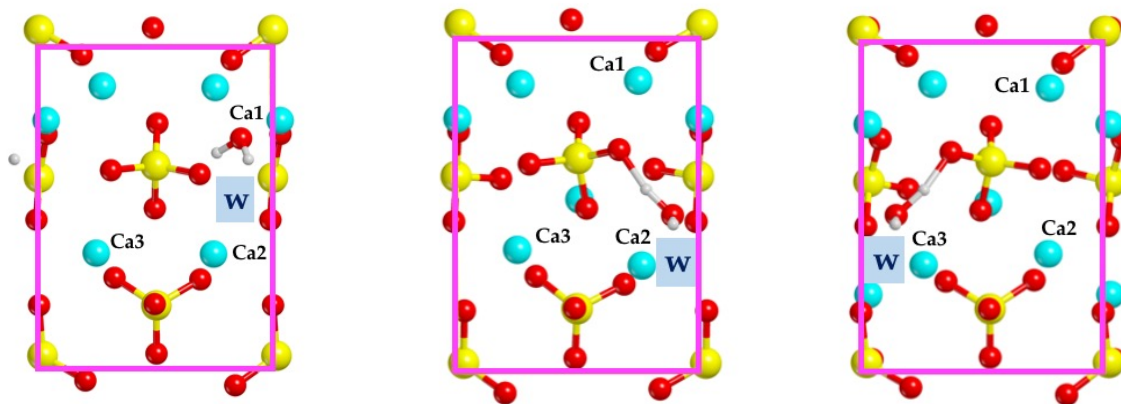
(c) Ca1-O 2.36   (d) Ca2-O 2.41   (e) Ca3-O 2.41

Figure 8: Physisorption of one water molecule at the (010) non-stoichiometic surfaces of CAp, top view. Panel (a) and (b) for the Ca-rich and (c) to (e) for the P-rich surface. Distances in Å.

Conversely, in the HA and CAp P-rich surface, the channel ion ($CO_3{}^{2-}$ or OH^-) is buried below two A-type layers, and therefore cannot be involved directly in water adsorption. The three CAp structures reported in Figures 8c, 8d and 8e confirm this hypothesis, showing the formation of a network of hydrogen bonds between water and phosphate groups. The computed interaction energy for the most stable (Figure 8e) is -115.0 kJ mol^{-1}, lower than the value of -135.4 kJ mol^{-1} reported for HA.[29]

20

Molecular dynamics simulations for water at CAp S (010)

We ran molecular dynamics simulations to elucidate the complex potential energy surface causing water dissociation on the S (010) surface. As reported in Figure 9, three 10 ps dynamics simulations were run on systems composed of the optimized CAp S (010) surface and one water molecule, with the molecule initially placed on each of three reactive calcium ions (Ca2A, Ca2B and Ca3). Figures 9a, 9b and 9c indicate that, independently of the initial configuration, within 10 ps the system evolves to a structure in which the water molecule is cleaved into a proton and an hydroxyl anion. The proton is transferred to an adjacent phosphate group (highlighted with the symbol w), while the hydroxyl occupies the center of the triangle defined by the three calcium ions. In this configuration, all three calcium ions, Ca2A, Ca2B and Ca3 concur in stabilizing the negative charge of the hydroxyl.

The B3LYP interaction energy calculated by full optimization of a frame of this molecular dynamics simulation yields a value of -186 kJ mol^{-1}, lower than the value of -245 reported for HA and higher than those reported for the non-stoichiometric surfaces.[25] It is hard to explain the relevant decrease of the adsorption energy moving from HA S (010) to the corresponding CAp surface. One reason may be the different local electric field exerted by CO_3^{2-} compared to OH^-, which decreases the ionic character of the Ca ions coordinating the OH^- group resulting from water cleavage. The other reason may be the increased steric hindrance of CO_3^{2-} compared to OH^-, which blocks the optimal geometry relaxation of the protonated PO_4^{3-} group.

(a) CAp (010): Ca2A

(b) CAp (010): Ca2B

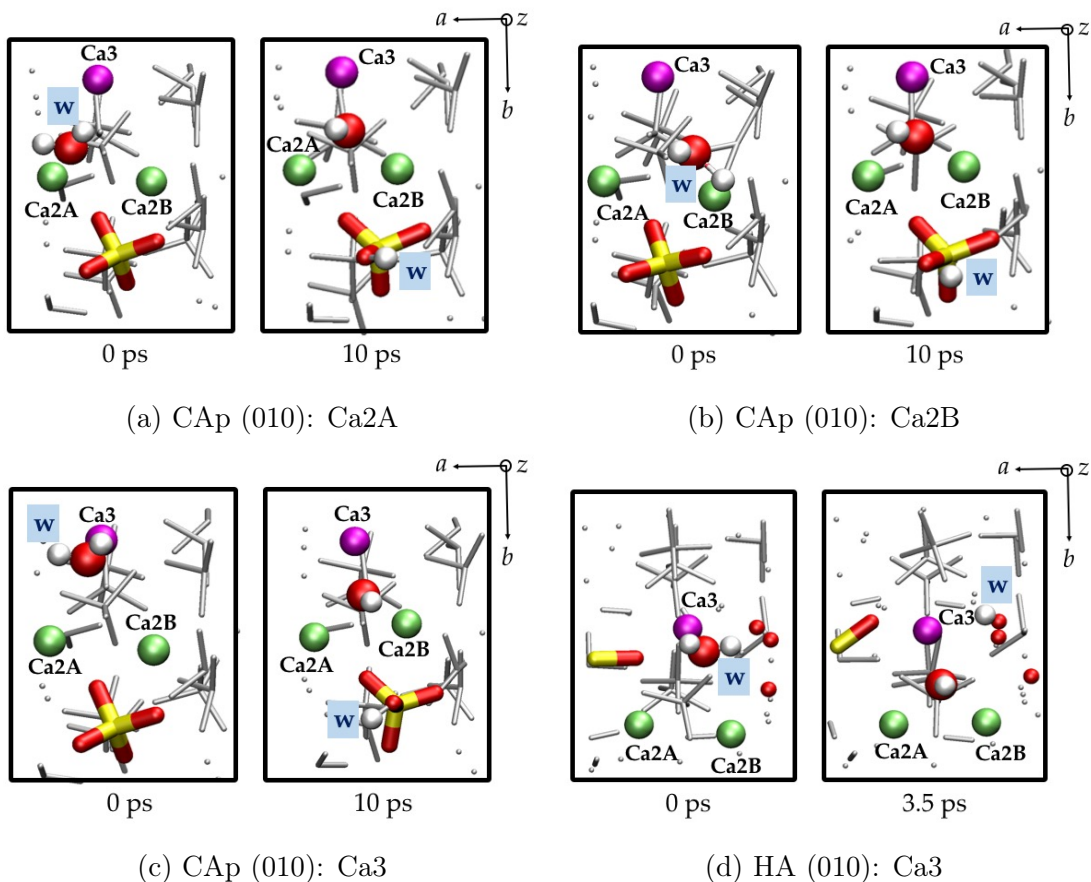(c) CAp (010): Ca3

(d) HA (010): Ca3

Figure 9: Molecular dynamics simulations of one water molecule on the stoichiometric (010) surface of HA and CAp. Green: Ca2 ions, purple: Ca3 ion.

To complete the dyamic picture, an analogous simulation has been run on the corresponding HA system. As shown in Figure 9d, the same reaction is observed within the same short time, yielding an equivalent symmetric configuration of the hydroxyl resulting from water cleavage; again, the hydroxyl ion is equidistant from Ca2A, Ca2B and Ca3. This indicates that carbonation does not partecipate directly this stage of water cleavage, and has an indirect influence mainly on the phosphate groups that accept the proton left by water. A more detailed analysis of interatomic distances along the molecular dynamics is reported in the ESI, Figures S11-S16.

Conclusions

In this work we compared some of the properties and reactivity of fully carbonated A-type carbonated apatite (CAp) surfaces, with those of hydroxyapatite (HA) as a reference. The A-type system envisages two OH- groups of the HA unit cell being substituted by one CO_3^{2-}. The resulting CAp shows around 6 wt% of carbonate content in line with the 2-8 wt% experimental datum for mammals bones. We adopted the hybrid B3LYP functional together with Gaussian-type basis functions, already adopted from previous works Ref[29]), to ensure proper comparability along different simulations involving the HA system.

We focused on the (001), (010) (both stoichiometric and non-stoichiometric) and (101) surfaces of HA and CAp systems, simulated within the finite slab model. The three classes of surfaces, exhibit quite different arrangments of the CO_3^{2-} groups within the slab as well as their exposure at the surfaces. The CO_3^{2-} group is localized in slightly different orientations within each surface slab due to its flat structure and rather high mobility in the former OH-channel. This, in turn, imparts a relatively small dipole moments across the slabs, in all cases larger than those computed for the corresponding HA surfaces. Nevertheless, surface energies for CAp are close to those for HA, but for the (001) case, in which CAp shows a higher value.

The vibrational features of the CO_3^{2-} group in the CAp surfaces are compared to the bulk features, to elucidate the effect of surface cut on the carbonate stretching vibrational frequencies. We found the stretching features of CO_3^{2-} to be sensitive to the local environment and map the position within the slab, the most buried ones resembling those of the CO_3^{2-} in the bulk crystal. A measure of the perturbation induced by the surface is the difference between the symmetric/antisymmetric CO_3^{2-} stretching compared to that of CO_3^{2-} in the bulk crystal, amounting to 86 cm^{-1}. For the external CO_3^{2-} group at the (001) CAp surface, it converges rapidly to the bulk value with the number of slab layers. For the (101) surface the value is as high as 260 cm^{-1}, revealing a rather asymmetric environment of the surface CO_3^{2-} compared to the bulk. This is also the case for both the stoichiometric and

Ca-rich (010) surfaces, the latter exhibiting higher deviations. For the P-rich (010) surface, the shift almost coincides with that of the bulk, as $CO_3{}^{2-}$ groups are buried within the framework of atoms even when close to the surface.

We probed the differences in surface features of CAp and HA by water adsorption at almost zero water coverage (one H_2O molecule per surface unit cell), in a first investigation of surface hydration. However preliminary, these result represent the first step towards the understanding of the behavior of carbonate apatite surfaces in a biological environment. We found water to be adsorbed on the same Ca ion sites as in HA. The comparison revealed a 17% increase in the binding energy of water at the CAp (001) surface. The CAp Ca-rich and P-rich (010) surfaces exhibit higher (50% increase)/lower(-20% decrease) interaction energies than HA, showing $CO_3{}^{2-}$ to significantly affect water adsorption, particularly for the Ca-rich case in which the carbonate is exposed at the surface. Both HA and CAp stoichiometric (010) surfaces react with water barrierlessly, with a 25% decrease in the interaction energy of CAp compared to HA. The final structural outcome is, however, very close to that observed at the HA (010) surface. Future work should address the case of higher water loading to reveal whether the local effects found at very low coverage will affect the water monolayer adsorption features.

Acknowledgement

Supporting Information Available

The following files are available free of charge.

- Filename: Graphical representation and CIF files of CAp surface models; details on the static and dynamic simulations.

This material is available free of charge via the Internet at `http://pubs.acs.org/`.

References

(1) Daculsi, G.; LeGeros, R. Z.; Heughebaert, M.; Barbieux, I. Formation of Carbonate-Apatite Crystals After Implantation of Calcium Phosphate Ceramics. *Calcif. Tissue Int.* **1990**, *46*, 20–27.

(2) Nagai, H.; Kobayashi-Fujioka, M.; Fujisawa, K.; Ohe, G.; Takamaru, N.; Hara, K.; Uchida, D.; Tamatani, T.; Ishikawa, K.; Miyamoto, Y. Effects of Low Crystalline Carbonate Apatite on Proliferation and Osteoblastic Differentiation of Human Bone Marrow Cells. *J. Mater. Sci. Mater. Med.* **2015**, *26*, 99.

(3) Hirota, M.; Hayakawa, T.; Ohkubo, C.; Sato, M.; Hara, H.; Toyama, T.; Tanaka, Y. Bone Responses to Zirconia Implants with a Thin Carbonate-Containing Hydroxyapatite Coating Using a Molecular Precursor Method. *J. Biomed. Mater. Res. B Appl. Biomater.* **2014**, *102*, 1277–1288.

(4) Liu, Y.; Zhou, Y.; Jiang, T.; Liang, Y.-D.; Zhang, Z.; Wang, Y.-N. Evaluation of the Osseointegration of Dental Implants Coated with Calcium Carbonate: an Animal Study. *Int. J. Oral Sci.* **2017**, *9*, 133–138.

(5) Germaini, M.-M.; Detsch, R.; Grünewald, A.; Magnaudeix, A.; Lalloue, F.; Boccaccini, A. R.; Champion, E. Osteoblast and Osteoclast Responses to A/B Type

Carbonate-Substituted Hydroxyapatite Ceramics for Bone Regeneration. *Biomed. Mater.* **2017**, *12*, 035008.

(6) Elliott, J. C.; Holcomb, D. W.; Young, R. A. Infrared Determination of the Degree of Substitution of Hydroxyl by Carbonate Ions in Human Dental Enamel. *Calcif. Tissue Int.* **1985**, *37*, 372–375.

(7) Suetsugu, Y.; Takahashi, Y.; Okamura, F. P.; Tanaka, J. Structure Analysis of A-Type Carbonate Apatite by a Single-Crystal X-Ray Diffraction Method. *J. Solid State Chem.* **2000**, *155*, 292–297.

(8) Fleet, M. E.; Liu, X. Location of Type B Carbonate Ion in Type A-B Carbonate Apatite Synthesized at High Pressure. *J. Solid State Chem.* **2004**, *177*, 3174–3182.

(9) Fleet, M. E.; Liu, X. Local Structure of Channel Ions in Carbonate Apatite. *Biomaterials* **2005**, *26*, 7548–7554.

(10) Fleet, M. E. Infrared Spectra of Carbonate Apatites: Evidence for a Connection Between Bone Mineral and Body Fluids. *Am. Mineral.* **2017**, *102*, 149–157.

(11) Deymier, A. C.; Nair, A. K.; Depalle, B.; Qin, Z.; Arcot, K.; Drouet, C.; Yoder, C. H.; Buehler, M. J.; Thomopoulos, S.; Genin, G. M.; *et al.*, Protein-Free Formation of Bone-Like Apatite: New Insights into the Key Role of Carbonation. *Biomaterials* **2017**, *127*, 75–88.

(12) Wopenka, B.; Pasteris, J. D. A Mineralogical Perspective on the Apatite in Bone. *Mater. Sci. Eng. C* **2005**, *25*, 131–143.

(13) Porter, A.; Patel, N.; Brooks, R.; Best, S.; Rushton, N.; Bonfield, W. Effect of Carbonate Substitution on the Ultrastructural Characteristics of Hydroxyapatite Implants. *J. Mater. Sci. Mater. Med.* **2005**, *16*, 899–907.
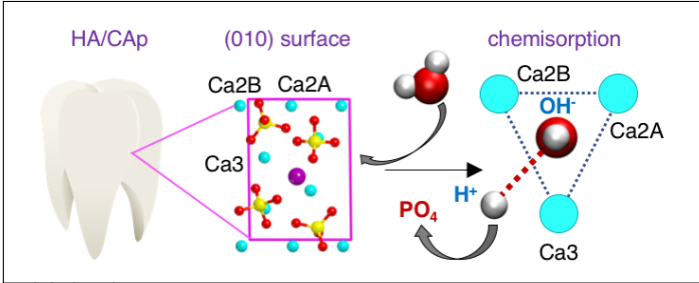
(14) Forien, J.-B.; Fleck, C.; Krywka, C.; Zolotoyabko, E.; Zaslansky, P. In Situ Compressibility of Carbonated Hydroxyapatite in Tooth Dentine Measured Under Hydrostatic Pressure by High Energy X-Ray Diffraction. *J. Mech. Behav. Biomed. Mater.* **2015**, *50*, 171–179.

(15) Choi, S.; Coonrod, S.; Estroff, L.; Fischbach, C. Chemical and Physical Properties of Carbonated Hydroxyapatite Affect Breast Cancer Cell Behavior. *Acta Biomater.* **2015**, *24*, 333–342.

(16) Germaini, M.-M.; Detsch, R.; Grünewald, A.; Magnaudeix, A.; Lalloue, F.; Boccaccini, A. R.; Champion, E. Osteoblast and Osteoclast Responses to A/B Type Carbonate-Substituted Hydroxyapatite Ceramics for Bone Regeneration. *Biomed. Mater.* **2017**, *12*, 035008.

(17) Nakamura, M.; Hiratai, R.; Hentunen, T.; Salonen, J.; Yamashita, K. Hydroxyapatite with High Carbonate Substitutions Promotes Osteoclast Resorption through Osteocyte-like Cells. *ACS Biomater. Sci. Eng.* **2016**, *2*, 259–267.

(18) Lala, S.; Ghosh, M.; Das, P. K.; Das, D.; Kar, T.; Pradhan, S. K. Structural and Microstructural Interpretations of Zn-Doped Biocompatible Bone-like Carbonated Hydroxyapatite Synthesized by Mechanical Alloying. *J. Appl. Cryst.* **2015**, *48*, 138–148.

(19) Prakash, M.; Lemaire, T.; Tommaso, D. D.; de Leeuw, N.; Lewerenz, M.; Caruel, M.; Naili, S. Transport Properties of Water Molecules Confined between Hydroxyapaptite Surfaces: A Molecular Dynamics Simulation Approach. *Appl. Surf. Sci.* **2017**, *418*, 296–301.

(20) Wu, H.; Xu, D.; Yang, M.; Zhang, X. Surface Structure of Hydroxyapatite from Simulated Annealing Molecular Dynamics Simulations. *Langmuir* **2016**, *32*, 4643–4652.

(21) Ren, F.; Lu, X.; Leng, Y. Ab Initio Simulation on the Crystal Structure and Elastic Properties of Carbonated Apatite. *J. Mech. Behav. Biomed. Mater.* **2013**, *26*, 59–67.

27

(22) Ulian, G.; Moro, D.; Valdrè, G. First-Principles Study of Structural and Surface Properties of (001) and (010) Surfaces of Hydroxylapatite and Carbonated Hydroxylapatite. *J. Appl. Cryst.* **2016**, *49*, 1893–1903.

(23) Ulian, G.; Moro, D.; Valdrè, G. Probing the Interaction of (001) Carbonated Hydroxylapatite Surfaces with Water: a Density Functional Investigation. *Micro Nano Lett.* **2018**, *13*, 4–8.

(24) Corno, M.; Busco, C.; Civalleri, B.; Ugliengo, P. Periodic Ab Initio Study of Structural and Vibrational Features of Hexagonal Hydroxyapatite $Ca_{10}(PO_4)_6(OH)_2$. *Phys. Chem. Chem. Phys.* **2006**, *8*, 2464–2472.

(25) Corno, M.; Busco, C.; Bolis, V.; Tosoni, S.; Ugliengo, P. Water Adsorption on the Stoichiometric (001) and (010) Surfaces of Hydroxyapatite: A Periodic B3LYP Study. *Langmuir* **2009**, *25*, 2188–2198.

(26) Corno, M.; Rimola, A.; Bolis, V.; Ugliengo, P. Hydroxyapatite as a Key Biomaterial: Quantum-Mechanical Simulation of its Surfaces in Interaction with Biomolecules. *Phys. Chem. Chem. Phys.* **2010**, *12*, 6309–6329.

(27) Chiatti, F.; Corno, M.; Ugliengo, P. Stability of the Dipolar (001) Surface of Hydroxyapatite. *J. Phys. Chem. C* **2012**, *116*, 6108–6114.

(28) Chiatti, F.; Corno, M.; Sakhno, Y.; Martra, G.; Ugliengo, P. Revealing Hydroxyapatite Nanoparticle Surface Structure by CO Adsorption: A Combined B3LYP and Infrared Study. *J. Phys. Chem. C* **2013**, *117*, 25526–25534.

(29) Chiatti, F.; Delle Piane, M.; Ugliengo, P.; Corno, M. Water at Hydroxyapatite Surfaces: the Effect of Coverage and Surface Termination as Investigated by All-Electron B3LYP-D* Simulations. *Theor. Chem. Acc.* **2016**, *135*, 54.

(30) Ulian, G.; Valdrè, G.; Corno, M.; Ugliengo, P. Periodic Ab Initio Bulk Investigation of Hydroxylapatite and Type A Carbonated Apatite with both Pseudopotential and All-Electron Basis Sets for Calcium Atoms. *Am. Mineral.* **2013**, *98*, 410–416.

(31) Ulian, G.; Valdrè, G.; Corno, M.; Ugliengo, P. The Vibrational Features of Hydroxylapatite and Type A Carbonated Apatite: A First Principle Contribution. *Am. Mineral.* **2013**, *98*, 752–759.

(32) Peccati, F.; Corno, M.; Delle Piane, M.; Ulian, G.; Ugliengo, P.; Valdrè, G. $CO_3{}^{2-}$ Mobility in Carbonate Apatite as Revealed by Density Functional Modeling. *J. Phys. Chem. C* **2014**, *118*, 1364–1369.

(33) Ulian, G.; Valdrè, G.; Corno, M.; Ugliengo, P. DFT Investigation of Structural and Vibrational Properties of Type B and Mixed A-B Carbonated Hydroxylapatite. *Am. Mineral.* **2014**, *99*, 117–127.

(34) Lee, C.; Yang, W.; Parr, R. G. Development of the Colle-Salvetti Correlation-Energy Formula into a Functional of the Electron Density. *Phys. Rev. B* **1988**, *37*, 785–789.

(35) Becke, A. D. Density-Functional Thermochemistry. III. The Role of Exact Exchange. *J. Chem. Phys.* **1993**, *98*, 5648–5652.

(36) Boys, S.; Bernardi, F. The Calculation of Small Molecular Interactions by the Differences of Separate Total Energies. Some Procedures with Reduced Errors. *Mol. Phys.* **1970**, *19*, 553–566.

(37) Simon, S.; Duran, M.; Dannenberg, J. J. How Does Basis Set Superposition Error Change the Potential Surfaces for Hydrogen-Bonded Dimers? *J. Chem Phys.* **1996**, *105*, 11024–11031.

(38) Vandevondele, J.; Krack, M.; Mohamed, F.; Parrinello, M.; Chassaing, T.; Hutter, J.

Quickstep: Fast and Accurate Density Functional Calculations Using a Mixed Gaussian and Plane Waves Approach. *Comput. Phys. Commun.* **2005**, *167*, 103–128.

(39) Lippert, G.; Hutter, J.; Parrinello, M. A Hybrid Gaussian and Plane Wave Density Functional Scheme. *Mol. Phys.* **1997**, *92*, 477–488.

(40) Goedecker, S.; Teter, M.; Hutter, J. Separable Dual-Space Gaussian Pseudopotentials. *Phys. Rev. B* **1996**, *54*, 1703–1710.

(41) Krack, M. Pseudopotentials for H to Kr Optimized for Gradient-Corrected Exchange-Correlation Functionals. *Theor. Chem. Acc.* **2005**, *114*, 145–152.

(42) Bussi, G.; Donadio, D.; Parrinello, M. Canonical Sampling Through Velocity Rescaling. *J. Chem. Phys.* **2007**, *126*, 014101.

(43) Jimenez-Izal, E.; Chiatti, F.; Corno, M.; Rimola, A.; Ugliengo, P. Glycine Adsorption at Nonstoichiometric (010) Hydroxyapatite Surfaces: A B3LYP Study. *J. Phys. Chem. C* **2012**, *116*, 14561–14567.

Graphical TOC Entry

TOC Graphic